Progress In Electromagnetics Research M, Vol. 55, 95–107, 2017

Design of Low-Pass Filter Using Meander Inductor and U-Form Hi-Lo Topology with High Compactness Factor for L-Band Applications

Wael Abd Ellatif[1, *] and Ahmed Boutejdar[2]

Abstract—In this paper, novel compact low-pass filters using Hi-Lo technique and meander method are proposed. Series of the proposed filters are designed by adding modifications along the microstrip line (meander inductor) and by using U-form topology. The size of the proposed filter can be reduced by 15% compared to the conventional filter while maintaining the optimal low-pass features. The compact meander LPF consists of two thin microstrip lines, which are connected with 50 Ω microstrip feed lines and a microstrip patch placed in the middle of the structure. The thin lines and the microstrip patch correspond to inductance and capacitance, respectively. The proposed meander Hi-Lo topology has been mounted on an RO4003 substrate with a relative dielectric constant $\varepsilon_r = 3.38$, thickness $h = 0.813$ mm and loss tangent 0.0027. The compact L-band low-pass structure has a size of $(0.263\lambda_g \times 0.175\lambda_g)$ where $\lambda_g = 57$ mm is the wavelength at the cutoff frequency 2.85 GHz. In addition to a good compactness, the structure exhibits a simple design, very low insertion loss in the passband (L-band) of less than 0.3 dB, and it achieves a wide rejection bandwidth with a 20 dB attenuation from 5.3 to 6.3 GHz. The excellent LPF characteristics are verified through simulations and measurements where a good consistency can be observed. Such compact filter structures are expected to be used in various microwave system applications.

1. INTRODUCTION

The rapid development of wireless communication systems has produced increasing research interest in features improvement and particularly in size miniaturization. The designs of low-pass filter topologies [1–3] with suppression of unwanted harmonics, sharp roll-off, ultrawide passband, low insertion loss, large rejection band, low fabrication tolerance and small occupied area are highly recommended for microwave circuits and modern telecommunication systems. Over these years, microstrip planar low-pass filters have been widely proposed as an approach solution to solve the most difficult technical challenges in microwave and wireless communication areas. One of the techniques that can be applied to planar LPF is employing a cascaded method in which the resonators are placed vertically or horizontally side by side [4–10]. The disadvantages of using this procedure appear in filter size and insertion loss, which not completely achieve the requirements of communication systems. Other researchers have used topologies based on DGS technique. Boutejdar et al., Ren, and Hejazi and Ali proposed filters using vertical and horizontal cascaded DGS-resonators [11–13] and thin slots [14, 15]. The disadvantages in such researches are the complicated DGS shapes, undesired coupling between the DGS resonators and large size of the proposed filter structures. In [16], the designed low-pass filter uses an interdigital structure between the symmetric rectangular couple capacitors, which not only reduces

Received 31 January 2017, Accepted 24 February 2017, Scheduled 21 March 2017

* Corresponding author: Wael Abd Ellatif (wael_abd_ellatif@yahoo.com).

[1] Electronics and Communications Engineering Department, Arab Academy for Science, Technology & Maritime Transport (AASTMT), Alexandria, Egypt. [2] Microwave and Communication Engineering, German Research Foundation DFG Bonn-Braunschweig, Germany.

the filter size but also provides the finite attenuation poles to suppress the undesired harmonics. The disadvantages in this work are the complicated design and fabrication due to the capacitor fingers, which are very close to each other and the emerging undesired electric coupling, which can negatively influence the filter response. Murphy et al. proposed a filter with stepped-impedance resonators (SIRs) as a technique with the aim of an ultra-wide stopband and a sharp transition domains [17]. Mokhtari et al. proposed a design methodology to these kind of filters using cascaded resonators on a coplanar structure [18]. However, in both proposed topologies, the disadvantages of large circuit size and presence of inaccurate results remain real challenge. In [8, 19], the candidated LPF employs defected microstrip structure (DMS) technique. DMS is achieved by etching uniform or nonuniform slit on the signal strip, and it exhibits the same frequency behavior as DGS. The DMS increases the electrical length and the corresponding inductance of the microstrip structure which influences the stopband filter features of the structure and leads to filter size minimization. The complicated design, discontinuities of edges and radiation losses are the main disadvantages of DMS, which hindered the researchers in the manufacturing process. Another technique called multilayer technique is used in [20] to improve the compactness of LPF. Nevertheless, the proposed topology suffers from a higher return loss in the passband. Although the multilayer technique provides a good compactness, a higher compactness factor with improved performance is also needed.

In this article, LPF structures using stepped impedance method (Hi-Lo) and meander technique are presented. The series starts with the design of conventional LPF, employing cascaded lumped elements L-C-L, which are placed on the substrate, behind each other along a straight line between the two ports. In order to minimize the size of this structure, a U-form topology is presented without any additional components. To improve the compactness of this topology and the structure's features, a meander form is added to the U microstrip line. This modification caused a shifting of the attenuation pole to lower frequency, which means minimization of the structure size. The proposed U-Hi-Lo LPF using internal and external meandered topologies has been designed on an RO4003 substrate with a thickness of 0.813 mm and relative dielectric constant of 3.38. The compact filter with internal meandered topology is designed, fabricated and measured. A comprehensive comparison between the proposed models is presented to show the attractive features of the proposed LPF model with very compact size.

2. ANALYSIS AND CIRCUIT MODEL OF THREE POLES HI-LO LOWPASS FILTER

Design of a 3-pole LPF based on Hi-Lo-technique at the cutoff frequency 1.3 GHz using the Chebyshev response having 0.1 dB ripple factor is desired. The prototype has the following normalized component values [21]: $g_1 = g_3 = 1.0316$, $g_2 = 1.1474$. The two series inductors and the shunt capacitor of the prototype are computed with $i = 1, 3$ & $J = 2$ using:

$$L_i = \frac{g_i Z_0}{\omega_c}, \quad C_j = \frac{g_j}{\omega_c Z_0} \quad \text{and} \quad Z_0 = 50\,\Omega \tag{1}$$

The LPF is realized on a substrate with $\varepsilon_r = 3.38$ and thickness $h = 0.813$ mm. The central capacitor of value $C = 2.8092$ pF is realized by the microstrip line section of length l_c having the characteristic impedance $24\,\Omega$ corresponding to width W_c. Two identical inductors correspond to the thin lines, each with characteristic impedance $93\,\Omega$, and are connected with the SMA ports as shown in Fig. 1. The value of the inductance is $L = 6.3148$ nH calculated using Eq. (1). Normally, the microstrip step-impedance sections are designed by using the following expressions [22],

$$\omega_c L = Z_{oL} \sin\left(\frac{2\pi l_L}{\lambda_{gL}}\right) + Z_{oC} \tan\left(\frac{\pi l_C}{\lambda_{gC}}\right) \tag{2}$$

$$\omega_c C = \frac{1}{Z_{oC}} \sin\left(\frac{2\pi\, l_C}{\lambda_{gC}}\right) + 2 * \frac{1}{Z_{oL}} \tan\left(\frac{\pi\, l_L}{\lambda_{gL}}\right) \tag{3}$$

Equation (2) shows that the series inductor L of the LPF is realized by the high impedance (Z_{oL}) microstrip of length l_L that supports guided wavelength λ_{gL}. The residual inductance of the low impedance (Z_{oC}) microstrip section of length l_C that supports guided wavelength λ_{gC} also contributes to the series inductance. Equation (3) shows the realization of capacitor by a low impedance line section of length l_C and the residual capacitance associated with the high impedance line. The two end inductive

reactances and the central capacitive reactance of the 3-pole prototype LPF are $\omega_c L_1 = \omega_c L_3 = 37.8\,\Omega$ and $(\omega_c C_2)^{-1} = 78.9\,\Omega$ at the cutoff frequency. The length of the inductance and capacitance can be computed using Equations (2) and (3). This way is more accurate and provide exact results, but the disadvantage is that the method takes into consideration the parasitic effect on high-impedance line and the open-end error, which makes the analysis more complicated and demands more time. In order to solve this problem, both effects will be compensated, which leads to approximate results. A simple and short way to calculate the dimensions of the proposed microstrip filter is introduced based on the Hi-Lo filter theory, $[Z]$ and $[ABCD]$ matrices. The lengths of the distributed elements can be calculated using the phase constant β and impedance Z_o. The $[ABCD]$ matrix can be written as:

$$\begin{pmatrix} A & B \\ C & D \end{pmatrix} = \begin{pmatrix} \cos(\beta l) & jZ_0 \cdot \sin(\beta l) \\ j/Z_0 \cdot \sin(\beta l) & \cos(\beta l) \end{pmatrix} \tag{4}$$

The relationship between $[Z]$ and $[ABCD]$ matrices is simply presented as follows:

$$Z_{11} = Z_{22} = \frac{A}{C} = -jZ_0 \cos(\beta l) \tag{5}$$

$$Z_{21} = Z_{12} = \frac{1}{C} = -jZ_0 \csc(\beta l) \tag{6}$$

with $\beta l < \pi/2$, the expressions in Eq. (7) and Eq. (8) correspond to the series inductance and the capacitance, respectively, as shown in Fig. 2. Based on these results, the T-network parameters are defined as follows:

$$Z_{11} - Z_{12} = jZ_0 \tan\left(\frac{\beta l}{2}\right) = Z_{22} - Z_{21} = j\frac{X}{2} \tag{7}$$

$$Z_{12} = -jZ_0 \csc(\beta l) = jB^{-1} \Rightarrow B = -\frac{1}{Z_0} \sin(\beta l) \tag{8}$$

In the case of $\beta l < \pi/4$ and very high Z_o, Equation (7) is calculated with the help of Taylor approximation as follows:

$$\tan(\beta l) = \frac{\sin\left(\frac{\beta l}{2}\right)}{\cos\left(\frac{\beta l}{2}\right)} \approx \frac{\beta l}{2} \tag{9}$$

$$Z_{11} - Z_{12} = jZ_h \frac{\beta l}{2} = j\frac{X}{2} \tag{10}$$

$$X = Z_h \beta l \tag{11}$$

$$B = 0 \tag{12}$$

The two Equations (11) and (12) result in a simple inductance as shown in Fig. 3.

The capacitive reactance can be extracted from expressions (13) and (14) with a very low Z_o and under the same previous conditions. This leads to shunt capacitance as shown in Fig. 4.

$$\frac{X}{2} \approx \Rightarrow \; X \approx 0 \tag{13}$$

$$B \approx -Y_l \beta l \approx \frac{-\beta l}{Z_l} \tag{14}$$

At $\omega = \omega_c$, the electrical length of the lines can be easily extracted with the aid of Eqs. (9) to (12) as follows:

$$j\omega_c L = jZ_h \beta_c l \tag{15}$$

$$\beta_c l_n = \frac{\omega_c L}{Z_h} = \frac{g_n Z_0}{Z_h} \tag{16}$$

$$-j\omega_c C = -j\frac{\beta_c l}{Z_l} \tag{17}$$

$$\beta_c l_n = \omega_c C Z_l = \frac{g_n Z_l}{Z_0} \tag{18}$$

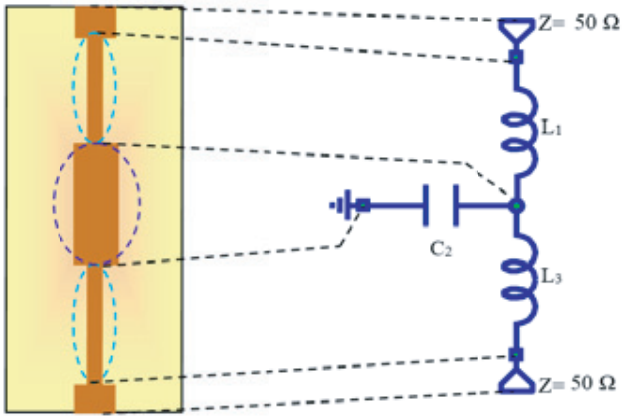

Figure 1. Layout of Hi-Lo LPF and its equivalent circuit.

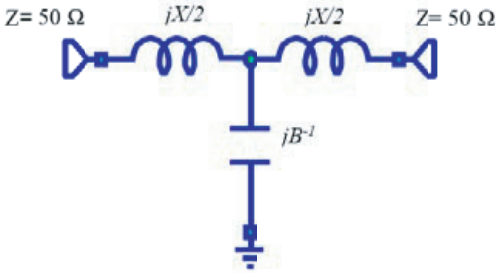

Figure 2. T-network of tree poles LPF.

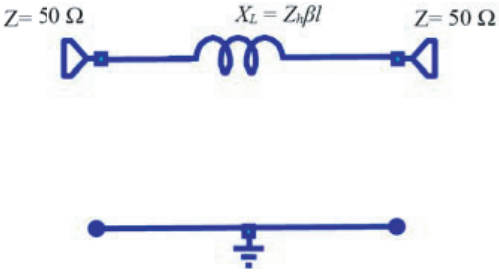

Figure 3. Equivalent circuit of high impedance line.

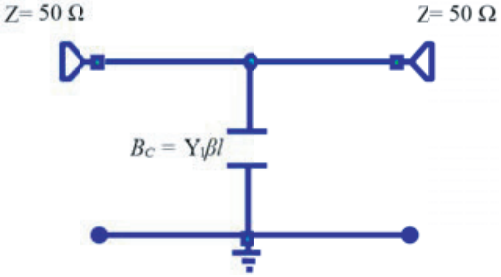

Figure 4. Equivalent circuit of low impedance line.

The filter has a cutoff frequency $f_c = 13\,\text{GHz}$ max. ripple along of passband $A_c = 01$ and $Z_{load} = Z_o = 50\,\Omega$. The element values g_i of the normalized 3rd order filter were selected from special table with various ripples [22]. Based on Eqs. (11) to (14), the lengths of the microstrip elements are defined. All dimensions of the Hi-Lo filter elements are calculated and listed in Table 1.

Table 1. Dimensions of the stepped impedance low-pass filter.

Element	Length (mm)		Width (mm)		Size (mm^2)
L_1	17	$0.135\lambda_g$	1	$0.008\lambda_g$	
C_2	15.3	$0.122\lambda_g$	5.2	$0.042\lambda_g$	50×20
L_3	17	$0.135\lambda_g$	1	$0.008\lambda_g$	$0.4\lambda_g \times 0.16\lambda_g$ $\lambda_g = 0.125\,\text{m}$
W_o			1.9	$0.015\lambda_g$	

3. DESIGN AND FABRICATION OF CONVENTIONAL HI-LO LOWPASS FILTER

As demonstrated previously, based on the filter theory [23] and using Richard and Kuroda transformations, the prototype values of inductors and capacitors are converted into the microstrip structure using Equations (2) and (3). Assumed values of high and low impedances are considered $93\,\Omega$ and $24\,\Omega$ respectively. After reduction of parasitic values, the actual lengths of different stubs are obtained as shown in Table 1. The simulations are carried out using an electromagnetic (EM)

simulator named as AWR Microwave Office [24]. A conventional 3rd order Chebyshev filter with -3 dB cutoff frequency at 1.3 GHz and attenuation of 0.1 dB in the passband has been designed on an RO4003 substrate with relative dielectric constant of $\varepsilon_r = 3.38$ and thickness of $h = 0.813$ mm. In this filter design, two high impedance thin lines (inductors) are from one side connected through 50 Ω feed lines to both SMA connectors and from the other side with the patch capacitor (low impedance).

Figure 5 presents the 3D-view of the Hi-Lo LPF and its dimensions. Fig. 7 shows the fabricated Hi-Lo LPF. The simulation results are depicted in Fig. 6 and show the response of a three-pole lowpass filter. The filter has a 3-dB cutoff frequency $f_c = 4.6$ GHz and a frequency pole $f_{0[8\,\mathrm{dB}]} = 7.5$ GHz. The disadvantage of this Hi-Lo structure is its larger size of $50 \times 20\,\mathrm{mm}^2$ and the translation of the desired cutoff frequency. As shown in Fig. 6 and Fig. 7, this kind of filter is not suitable for a modern communication system due to the large size of the topology and poor stopband response.

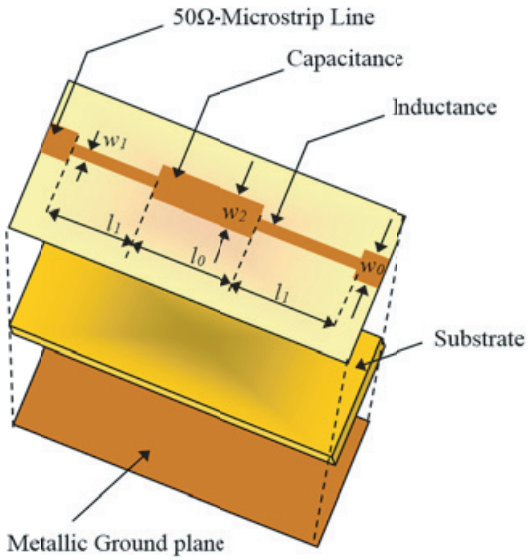

Figure 5. Layout of the conventional Hi-Lo low-pass filter.

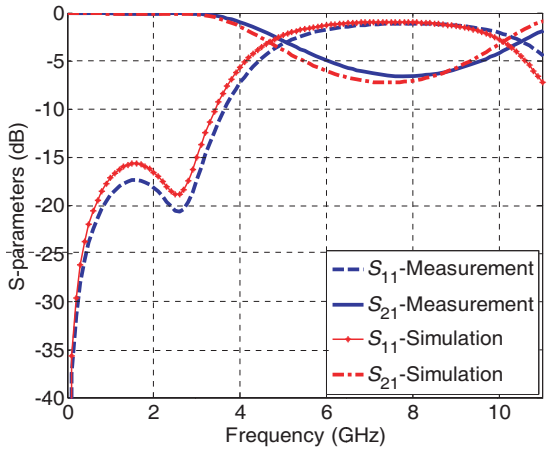

Figure 6. Measured and simulated S-parameters of conventional Hi-Lo LPF.

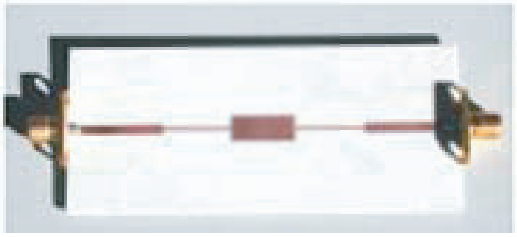

Figure 7. Photograph of fabricated conventional Hi-Lo low-pass filter.

4. DESIGN AND FABRICATION OF HI-LO LOW-PASS FILTER USING STUB CAPACITOR

The disadvantages of the structure shown in Fig. 6 are the scattering parameter S_{21}, which is not sharp enough in the transition region, and the rejection bandwidth of -10 dB is not achieved which leads to a poor stopband as shown in Fig. 7. Thus, the presented results are not as satisfying as expected. Therefore, the demand of such topologies with enhanced features still exists. Another filter topology, with the same dimensions as the conventional Hi-Lo-filter, has been designed and optimized. The idea

of the new filter topology based on rotating the patch capacitor by $\pi/2$ (open-circuited stub) compared to the conventional LPF is shown in Fig. 8. The rotated stub capacitor has a length of $l_{01} = 12\,\text{mm}$ and width of $w_{01} = 6.63\,\text{mm}$. Because of rotation of the patch capacitor, the dimensions of the patch capacitor are modified so that the filter keeps the same filtering conditions and features. The stub capacitor based LPF is designed and optimized at a cutoff frequency 3.4 GHz, and is simulated and fabricated on a Rogers RO4003 substrate of relative permittivity $\varepsilon_r = 3.38$, size $50 \times 20\,\text{mm}^2$, thickness $h = 0.813\,\text{mm}$ and loss tangent $\tan\delta = 0.0027$. Fig. 10 shows the fabricated prototype of the LPF using stub capacitor. A comparison between measured results of the two Hi-Lo LPF topologies (Conventional and stub) is depicted in Fig. 9. As expected, the response of stub capacitor based LPF in the passband has the same cutoff frequency $f_c = 3.4\,\text{GHz}$ with an improved value of attenuation pole which reaches $-32\,\text{dB}$ instead of $-8\,\text{dB}$ of conventional LPF as clearly shown in Fig. 10.

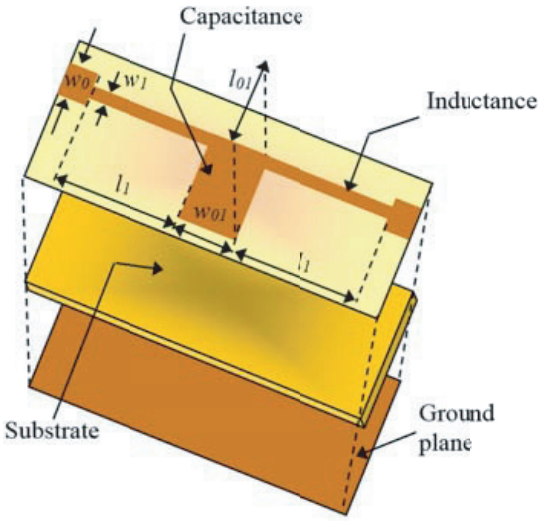

Figure 8. 3D-view of the conventional Hi-Lo lowpass filter using stub capacitor.

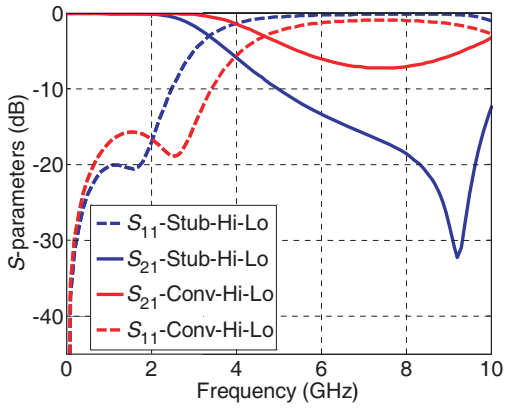

Figure 9. Measured results of both Hi-Lo low-pass filters.

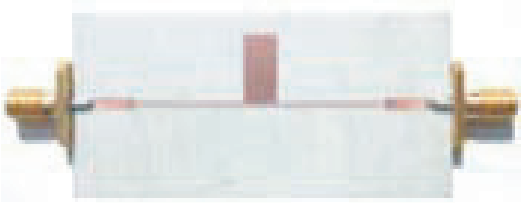

Figure 10. Photograph of fabricated Hi-Lo low-pass filter using stub capacitor.

5. DESIGN OF HI-LO LOW-PASS FILTER USING MEANDER SHAPE AS HIGH IMPEDANCE LINE

In order to improve the passband and compactness of the proposed stub low-pass filter, two meander forms are inserted on both sides of the patch capacitor as shown in Fig. 11. Both the meander inductors are directly connected with the SMA connectors through two $50\,\Omega$ microstrip lines. The structure is mounted on a Rogers RO4003 substrate with relative dielectric constant of 3.38 and thickness of 0.813 mm.

Figure 12 depicts the simulation results of this meander LPF, and it can be noticed that the scattering parameters show relative good results since the return loss in the passband reaches

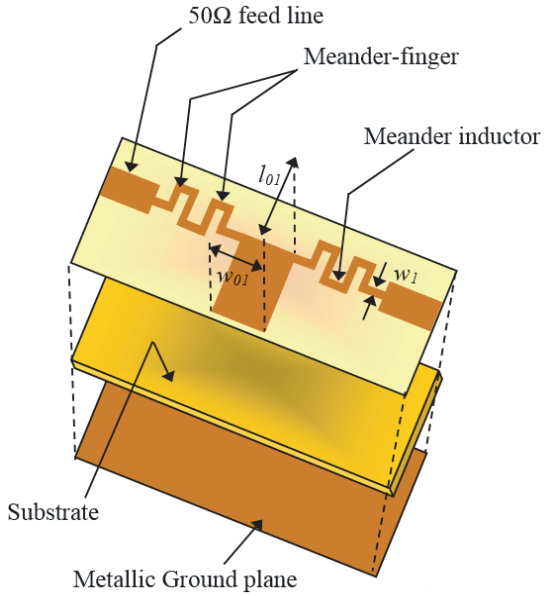

Figure 11. 3D-view of Hi-Lo low-pass filter using meander shapes.

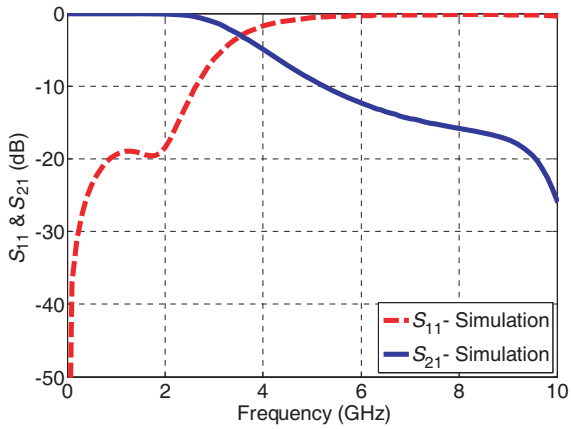

Figure 12. S-parameters of the Hi-Lo low-pass filter using meander shapes.

approximately −20 dB, which could not be achieved in the previous topologies. However, both cutoff and attenuation pole frequencies are shifted to the high-frequency range. The unique physical explanation for this behaviour is that the edges between the meander neighbour fingers lead to an undesired close magnetic coupling, which in turn causes a reduction of the inductance and thus moving both characteristic frequencies to the high-frequency range. As can be seen from the results in Fig. 12, the insertion loss from DC to 3 GHz is less than 0.2 dB and the attenuation pole located at around 11 GHz. The rotated stub capacitor has a length $l_{01} = 12$ mm and width $w_{01} = 6.63$ mm, while all other dimension values remain identical to the previous values of Hi-Lo filter.

6. DESIGN OF COMPACT HI-LO LOWPASS FILTER USING U-FORM TOPOLOGY

Due to the unsatisfactory results of the meander LPF with stub capacitor, a new technique is introduced to the Hi-Lo LPF by using U-form topology. Fig. 13 shows the schematic view of the U-Hi-Lo LPF. The structure consists of the same components as in the conventional Hi-Lo filter. However, the two SMA connectors are not placed at the extremities of the filter structure but located side by side in U-form on extremity of the structure as shown in Fig. 13. Using U-topology can reduce the size to 15% compared to the previous structures. It can be noticed from scattering parameters in Fig. 14 that the insertion and return losses are improved. The passband remains constant while both cutoff frequency and attenuation pole are clearly shifted to the low-frequency range. The characteristic frequencies can be easily controlled in the L-band and S-band. The U-Hi-Lo LPF is simulated and optimized using AWR and designed using a Rogers RO4003 substrate with the same simulation parameters as before. As shown in Fig. 14, the filter has cutoff and transmission zero at 3.5 GHz and 7.3 GHz, respectively.

7. IMPROVEMENT OF HI-LO LOWPASS FILTER USING U-FORM AND EXTERNAL-MEANDER SHAPE

In order to improve the filter features such as compactness and roll-off transition, a new filter design based on a combination technique of U-Hi-Lo-structure and meander technique is proposed. Fig. 15 shows a three-dimensional view of this new topology-idea with the aim of increasing the compactness factor of this structure without introducing any extra components. The external-meander shapes are placed between the 50 Ω feed line and the stub-capacitor. Fig. 16 shows a shift of the characteristic

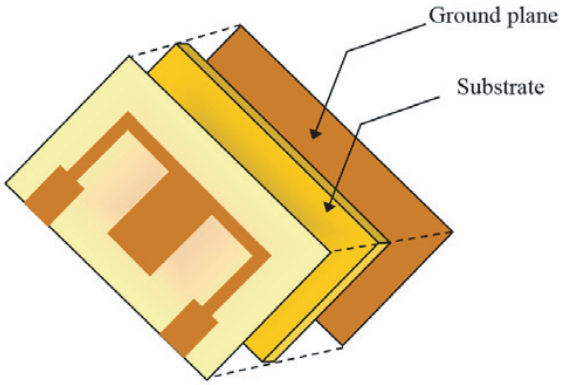

Figure 13. 3D-view of the Hi-Lo lowpass filter in U-form.

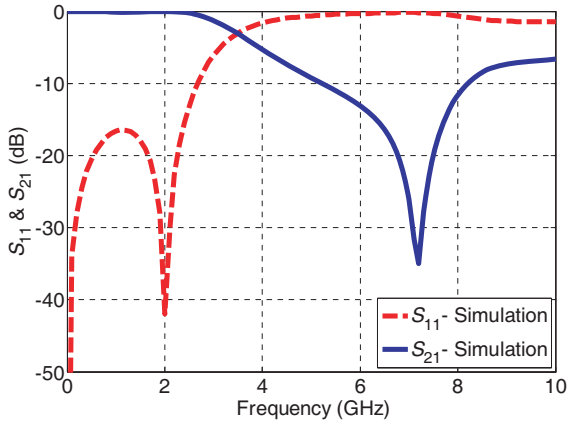

Figure 14. Simulation results of Hi-Lo lowpass filter in U-form.

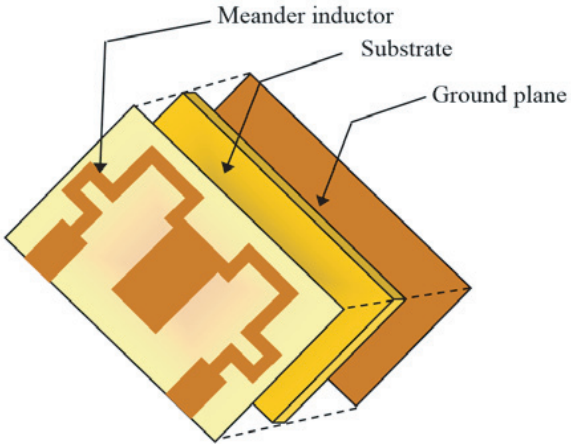

Figure 15. 3D-view of the U-Hi-Lo LPF using external meander shape.

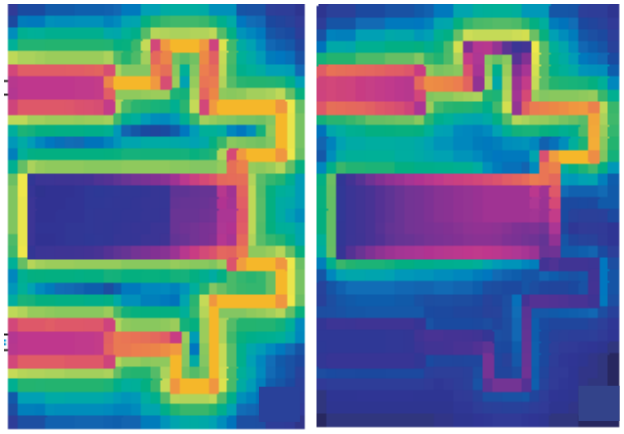

Figure 16. Electric field distribution. (a) $f = 2\,\text{GHz}$, (b) $f = 6.9\,\text{GHz}$.

frequencies in the direction of low-frequency domain. Consequently, the control of the filter response can be feasible, which means that the compactness can be easily achieved. To validate our approach, a meandered-U-low-pass filter is modeled and optimized to operate at 3.5 GHz using commercial 3D full-wave electromagnetic simulation tool (HFSS) [25]. The filter is designed and simulated using Rogers RO4003 substrates with relative dielectric constant of 3.38, thickness of 0.813 mm and loss tangent of $\tan\delta = 0.0027$. To avoid the disadvantages of using the meander Hi-Lo LPF, which were previously observed due to the undesired EM couplings generated between the fingers of the added meander shape, a new idea is applied to the meander shape where the new external meander shape is designed with enough distance between its fingers. In order to demonstrate the behaviour of surface electric field and its relationship with the EM-simulation results of the proposed U-meander LPF, the field distribution is simulated at two different frequencies in the passband and stopband. Fig. 16(a) depicts the field distribution in the passband region at the frequency of 2 GHz. At this frequency, almost the total RF energy is distributed from the input port to the output port using the external meander arms, which are connected with the patch capacitor and with SMA connectors. A negligible electric energy appears around the edge of the patch capacitor which confirms that the filter is in the passband state, and the metal strip has inductive behaviour.

Finally, it can be easily observed that the quasi-ring structure corresponds to a parallel LC-

resonator. At the attenuation pole ($f = 6.9\,\text{GHz}$), the electric energy is distributed along the left meander-arm between the stub capacitor and the input while no energy appears along the opposite meander-arm as shown in Fig. 16(b), which indicates that the structure is in the stopband state, and the transfer function behaves as transmission zero. Fig. 17 shows the response of the U-meander-Hi-Lo LPF, and it can be noticed that the scattering parameters have cutoff and attenuation pole at 3.5 GHz and 6.9 GHz respectively. Also, tt can be observed that the roll-off rate for this structure is $\xi_{\text{external}} = 6.8\,\text{dB/GHz}$ which is better than the rates of the previous structure shown in Fig. 13 ($\xi_{\text{U-form}} = 5.3\,\text{dB/GHz}$). The roll-off rate can be calculated using the following equation.

$$\xi = \frac{\alpha_{\max} - \alpha_{\min}}{f_0 - f_c} \tag{19}$$

where $\alpha_{\max}$ is the 20 dB attenuation point; $\alpha_{\min}$ is the 3 dB attenuation point; f_o is the 20 dB stopband frequency; f_c is the 3 dB cutoff frequency.

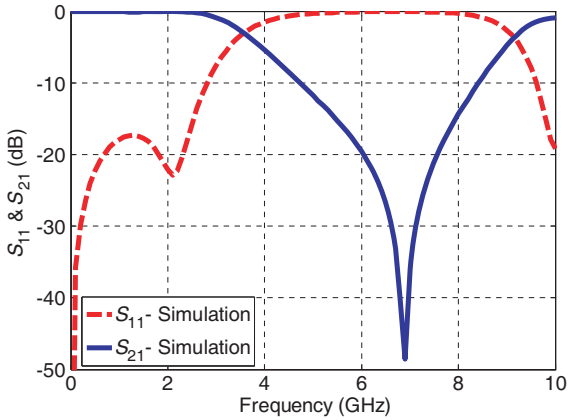

Figure 17. *S*-parameters of U-Hi-Lo low-pass filter using external meander shapes.

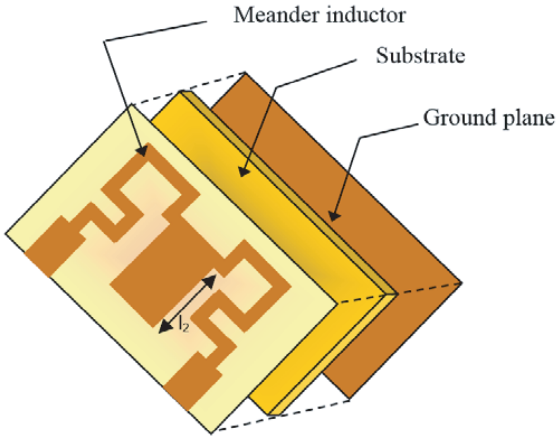

Figure 18. Layout of the proposed Hi-Lo LPF using internal-meander shape.

8. DESIGN OF COMPACT U-HI-LO LOW-PASS FILTER USING INTERNAL-MEANDER SHAPE

The idea of this study is focused on how to obtain a compact structure using minimal components and simple topology. For that purpose, an alternative U-meander LPF with internal fingers is designed and optimized. Fig. 18 shows a layout of the alternative structure. The modification is accomplished at the level of the meander-finger so that the structure is shrunk compared to the previous topologies. The meander-finger is rotated by 180°, thus the width of the structure is reduced by 13%. Consequently, the size of the filter becomes more compact than before, as depicted ub Fig. 18.

To validate our approach, the proposed meander-U-low-pass filter is simulated, optimized, and fabricated to operate in the L-band. The simulation results are presented in Fig. 19, and it can be noticed that the cutoff frequency is at 2.85 GHz while the attenuation pole is located at 6.3 GHz. A parametric study is carried out in order to investigate the influence of changing the length of stub-capacitor on the scattering parameters. Fig. 20 depicts the different simulation results of the proposed filter for different lengths of the patch capacitor. As shown in Fig. 20, all Hi-Lo dimensions are kept constant while the length of the stub capacitance is varied from 1 to 7 mm. This causes a shift of the attenuation pole and cutoff frequency to a lower frequency. Hence, the cutoff frequencies are shifted from 3.4 to 2.5 GHz and the transmission zeros from 9.9 to 5.9 GHz, which confirm the ability of the proposed filter to be compact in size. Fig. 21 shows the schematic view of the proposed internal meander LPF with all optimized dimensions based on the aforementioned parametric study. The proposed LPF is fabricated on Rogers RO4003 substrates with relative dielectric constant of 3.38, thickness of 0.813 mm and loss tangent of $\tan\delta = 0.0027$ with an overall size $15 \times 10\,\text{mm}^2$ as shown in Fig. 22. The impedance

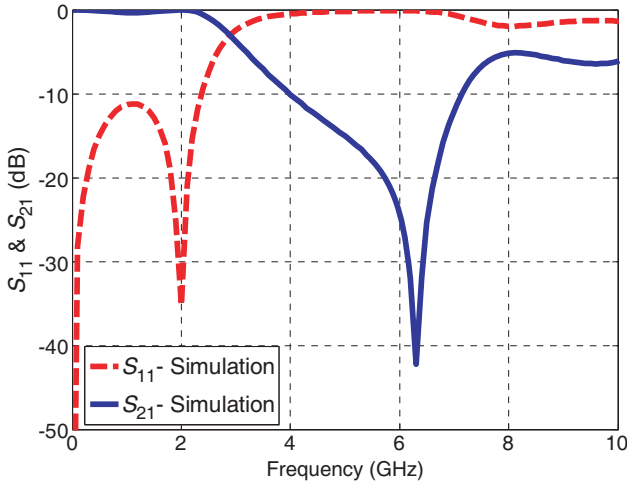

Figure 19. S_{11} and $S_{21}$of the proposed Hi-Lo LPF using internal-meander shape.

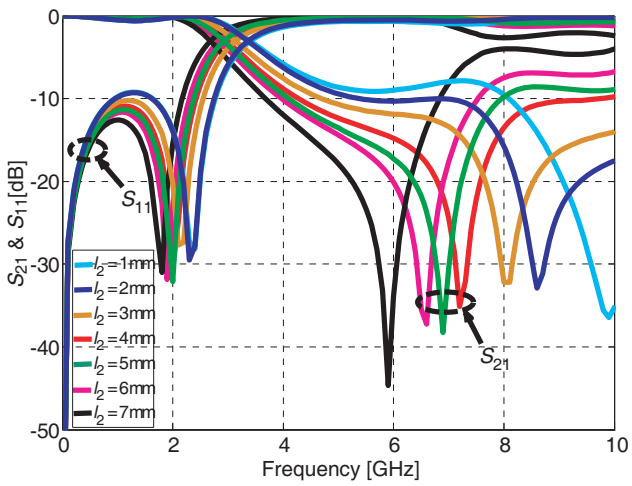

Figure 20. Simulated S-parameters versus the length of stub capacitor.

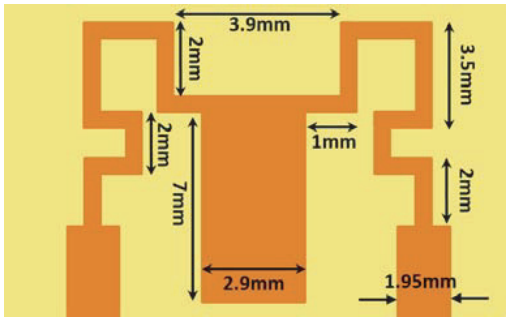

Figure 21. Schematic view of the internal-meander U-form LPF with all dimensions.

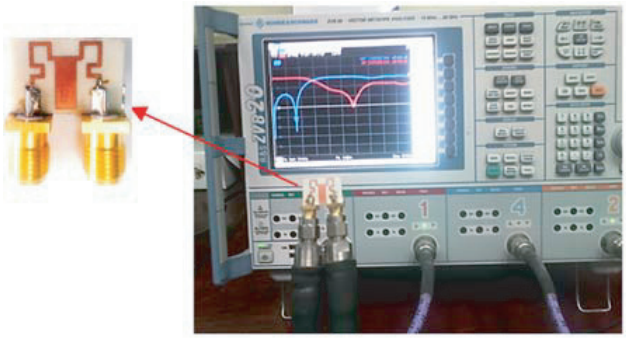

Figure 22. 3D-view of the proposed internal-meander LPF connected to VNA.

characteristics are measured using R&S ZVB 20 network-analyser. Fig. 23 shows a comparison between simulated and measured results of the proposed model with the optimized dimensions. The simulation is carried out using HFSS software in order to verify the experimental results [25].

As expected, the measured results of the fabricated prototype show that the insertion loss is less than 0.3 dB over the entire passband, and the bandwidth of the stopband at −20 dB is from 5.3 to 6.3 GHz while at −10 dB, the width of stopband is from 4.1 to 6.8 GHz as shown in Fig. 23. The results show clearly that both characteristic frequencies are shifted toward the lower side due to changing the angle of meander-fingers. The cutoff frequency is shifted from 3.5 GHz to 2.85 GHz, while the transmission zero is shifted from 6.9 GHz to 5.9 GHz. It can be observed that the idea of inverting the meander finger causes a significant shift of the characteristic frequencies and thus increases the roll-off rate (ξ_{internal}) = 7.17 dB/GHz compared to the achieved rate for the external meander LPF. Consequently, an improvement of the compactness is achieved. So, the fabricated filter looks attractive for L-band radar satellite due to its good performance and the overall physical size reduction. The electric field distribution is investigated in order to examine the performance of the proposed internal meander LPF as shown in Fig. 24. It is clear that the filter operates effectively since the overall field is uniformly distributed over the structure. The electric field distribution is simulated at two different frequencies, one in the passband (1.7 GHz) and the other in the stopband (6 GHz). At 1.7 GHz, the electric field is almost distributed from the input to the output through the internal meander arms which confirms that the filter is in the passband state as shown in Fig. 24(a) while at the 6 GHz, the energy is focused on the input zone between the stub capacitor and the SMA connector. This state

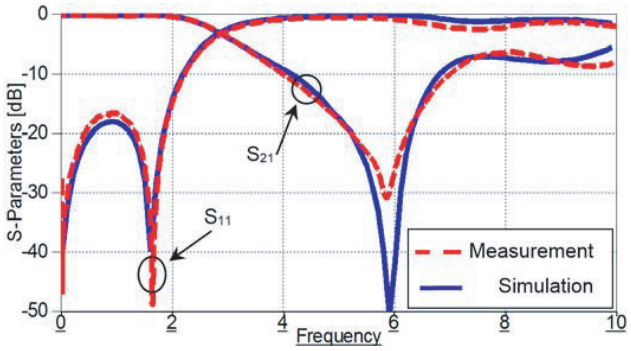

Figure 23. Simulated and measured S-parameters of the proposed Hi-Lo LPF.

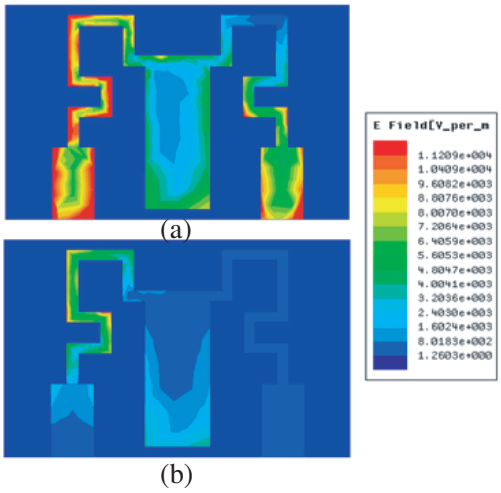

Figure 24. Electric field distribution: (a) $f = 1.7$ GHz, (b) $f = 6$ GHz.

declares that the behaviour of the structure is characterized by a stopband at this attenuation pole as shown in Fig. 24(b).

9. SUMMARY OF SCATTERING RESPONSES FOR DIFFERENT INVESTIGATED FILTERS

In this section, a simple comparison among different investigated topologies is carried out in order to demonstrate the main features and advantages of each designed structure. As shown in Fig. 25, the insertion loss of Hi-Lo, U-Hi-Lo, external meander and internal meander LPF are compared under the same filter conditions. It can be noticed that all structures present the same passband where the cutoff frequencies of all topologies are almost the same at 3.5 GHz except that the cutoff frequency for the internal meander-Hi-Lo topology is identical at 2.85 GHz. The internal meander-Hi-Lo and U-Hi-Lo structures have identical −20 dB stopband width, which is approximately equal to 1 GHz, while the external meander-Hi-Lo and stub-Hi-Lo structures shown early have the same value of −20 dB stopband width, which is approximately equal to 1.5 GHz. The values of the four transmission zeros of stub-Hi-Lo, U-Hi-Lo, external meander and internal meander LPF are 9.3, 7.3, 6.9 and 5.9 GHz, respectively.

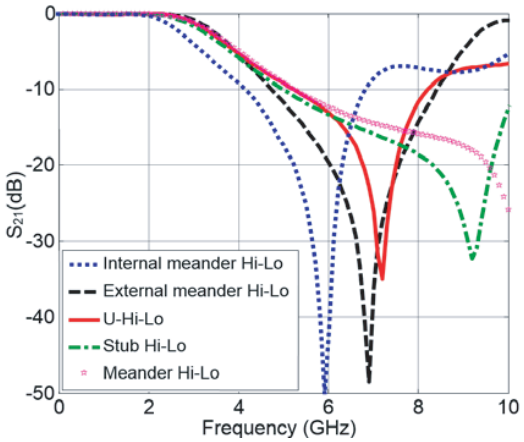

Figure 25. Performance comparison of different filter topologies.

Table 2. Comparison between the parameters of investigated filters.

Filter Topology	f_c (GHz)	f_o (GHz)	$\Delta f_{20\,\mathrm{dB}}$ (GHz)	ξ (dB/GHz)	Size (mm^2)
Conventional Hi-Lo-$_{8\,\mathrm{dB}}$	4.6	7.5	2	1.66	50×20
Stub Hi-Lo	3.4	9.3	1.2	3.50	50×20
Meander Hi-Lo	3.4	11	0.8	2.83	50×20
U-Hi-Lo	3.5	7.3	0.9	5.31	15×10
External meander Hi-Lo	3.5	6.9	1.5	6.80	15×10
Internal meander Hi-Lo	2.85	5.9	1.0	7.17	15×10

Table 2 shows a performance comparison among different topologies, and it lets us conclude that the last proposed topology (internal meander LPF) is the most compact model ($15 \times 10\,\mathrm{mm}^2$) with the highest roll-off rate factor ($\xi = 7.17\,\mathrm{dB/GHz}$). Such a filter topology can be a good candidate in several radar and wireless communication systems operating in L-band due to its compactness, good passband and high roll-off rate.

10. CONCLUSION

By utilizing Hi-Lo method and meander technique, a compact L-band low pass filter is developed and introduced. The proposed LPF is a combination of U-Hi-Lo topology and meander technique to improve filter features and increase the compactness factor. The proposed structure has a very compact size of ($15 \times 10\,\mathrm{mm}^2$) and can achieve a passband from DC to 2.85 GHz with -20 dB stopband from 5.3 to 6.3 GHz. Compared to the series of presented topologies in the literature, the proposed internal meander U-Hi-Lo LPF exhibits a relatively flat passband, sharp roll-off transition and compact size, which can be easily integrated with other devices. These attractive features make the proposed LPF suitable for employing in advanced L-band Radar and modern wireless communication systems.

REFERENCES

1. Boutejdar, A., "Design of wide stop band L-band LPF based on DMS-DGS-technique for radar applications," *International Journal of Microwave Science and Technology*, 2015.
2. Parui, S. K. and S. Das, "Modeling of modified split-ring type defected ground structure and its application as bandstop filter," *Radio Engineering Journal*, Vol. 18, No. 2, 149–154, June 2009.
3. Boutejdar, A., A. El-Sherbini, and A. S. Omar, "Method for widening the reject-band in lowpass/bandpass filters by employing coupled C-shaped defected ground structure (DGS)," *IET Microwaves, Antennas & Propagation*, Vol. 17, No. 12, 1405–1408, December 2008.
4. Liu, H., Z. Li, X. Sun, and J. Mao, "A novel photonic band-gap microstrip structures for lowpass filters of wide stop-band," *Microwave and Optical Technology Letters*, Vol. 37, 470–472, 2003.
5. Boutejdar, A., "Design of broad-stop band low pass filter using a novel quasi-Yagi-DGS-resonators and metal box-technique," *Microwave and Optical Technology Letters*, Vol. 56, No. 3, 523–528, 2014.
6. Yang, J. and W. Wu, "Compact elliptical low-pass filter using defected ground structure," *IEEE Wireless Comp. Lett.*, Vol. 18, No. 9, 2008.
7. Lim, J. S., C. S. Kim, D. Ahn, Y. C. Jeong, and S. Nam, "Design of low pass filter using defected ground," *IEEE Trans. Microwave Theory and Techniques*, Vol. 53, No. 8, 2539–2545, 2005.
8. Boutejdar, A., N. M. Eltabit, A. A. Ibrahim, and E. P. Burte, "Design of wide stop band L-band LPF based on DMS-DGS-technique for radar applications," *International Journal of Microwave Science and Technology*, Vol. 2015, Article ID 101602, 7 pages, Hindawi Publishing Corporation, 2015.

9. Tu, W. H. and K. Chang, "Compact microstrip low-pass filter with sharp rejection," *IEEE Microwave and Wireless Components Letters*, Vol. 15, No. 6, 404–406, June 2005.
10. Boutejdar, A., W. Abd Ellatif, A. A. Ibrahim, and M. Challal, "A simple transformation from lowpass to bandpass filter using a new quasi-arrow head defected ground structure resonator and gap-J-inverter," *Microwave and Optical Technology Letters*, Vol. 58, No. 4, 947–953, 2016.
11. Boutejdar, A., "A new approach to design compact tunable BPF starting from simple LPF topology using a single T-DGS-resonator and ceramic capacitors," *Microwave and Optical Technology Letters*, Vol. 58, No. 5, 1142–1148, 2016.
12. Ren, L.-Y., "Quad-band bandpass filter based on dual-plane micro- strip/DGS slot structure," *Electron. Lett.*, Vol. 46, 691–692, 2010.
13. Hejazi, Z. M. and Z. Ali, "Multiband bandpass filters with suppressed harmonics using a novel defected ground structure," *Microwave and Optical Technology Letters*, Vol. 56, No. 11, 2726–2731, 2014.
14. Boutejdar, A., A. Ramadan, M. Makkey, and A. S. Omar, "Design of compact microstrip lowpass filters using a U-shaped defected ground structure and compensated microstrip line," *Proceedings of the 36th European Microwave Conference*, 267–270, 2006.
15. Abdel-Rahman, A. B., A. K. Verma, A. Boutejdar, and A. S. Omar, "Control of bandstop response of Hi-Lo microstrip low-pass filter using slot in ground plane," *IEEE Trans. Microwave Theory and Techniques*, Vol. 52, No. 3, 1008–1013, 2004.
16. Boutejdar, A., M. Challal, A. Omar, E. Burte, R. Mikuta, and A. Azrar, "A novel band-stop filter using octagonal-shaped patterned ground structures along with interdigital and compensated capacitors," *ACES Journal — The Applied Computational Electromagnetics*, Vol. 26, No. 10, July 2011.
17. Murphy, L., M. Yazdani, and E. Arvas, "Ultra-wide stopband in a compact low pass filter using stepped impedance resonators and novel techniques," *2012 IEEE International Conference on Ultra-Wideband*, 92–94, Syracuse, NY, 2012.
18. Mokhtaari, M., J. Bornemann, and S. Amari, "Coupling-matrix design of dual/triple-band uni-planar filters," *IEEE MTT-S Int. Microw. Symp. Dig.*, 515–518, San Francisco, CA, June 2006.
19. Xiao, J.-K., W.-J. Zhu, and J.-S. Fu, "New bandstop filter using simple defected microstrip structure," *Microwave Journal*, Vol. 11, 2011.
20. Boutejdar, A. and W. A. E. Ali, "Improvement of compactness of low pass filter using new quasi-yagi-DGS-resonator and multilayer-technique," *Progress In Electromagnetics Research C*, Vol. 69, 115–124, 2016.
21. Pozar, D. M., *Microwave Engineering*, 3rd Edition, John Wiley & Sons, Inc., New York, 2005
22. Hong, J. S. and M. J. Lancaster, *Microstrip Filters for RF/Microwave Applications*, J. Wiley & Sons, Inc., New York, 2001.
23. Yang, J., "Design of RF filter based on Richards transform and Kuroads rules," *Journal of Taizhou University in China*, Vol. 28, No. 3, 41–46, 2006.
24. AWR's Microwave Office software, Inc., http://web.awrcorp.com/.
25. Ansoft High Frequency Structure Simulator (HFSS), Ver. 13, Ansoft Corporation, 2010.